Propulsion and Power Research 2013;2(1):38–49

http://ppr.buaa.edu.cn/

Propulsion and Power Research

www.sciencedirect.com

ORGINAL ARTICLE

# Stress and deformation of rocket gas turbine disc under different loads using finite element modelling

**Amr Elhefny, Guozhu Liang***

*School of Astronautics, Beihang University, Beijing 100191, China*

Received 27 September 2012; accepted 23 October 2012
Available online 21 March 2013

**KEYWORDS**

Rocket turbine;
Turbine disc;
Stress;
Deformation;
Finite element (FE)

**Abstract** Gas turbine discs have numerous applications in the aerospace industry, such as in liquid rocket engines. In this study, the stresses and deformations of a turbine disc were studied. The goal was to highlight the stress and deformation distribution to assist in the design of a disc as well as to demonstrate the importance of using finite element (FE) analysis in simulating an actual design case. Then, to present the real model, a two-dimensional (2D) axisymmetric model for a non-uniform disc was analysed using FE analysis. The stresses and deformations developed as a result of the disc operating conditions at high rotational speeds and thermal gradients were evaluated using two types of heat transfer modes—conduction and convection, taking into consideration the material behaviour at elevated temperatures. The FE model revealed that the weight of the disc should be reduced optimally by using a non-uniform thickness because this results in a huge increase in the applied stresses. The greatest stresses in the disc result from the thermal load caused by conduction, and they are located at the centre of the disc. In addition, an analytical method was used to evaluate and predict the stresses along the disc, and it gave a good estimate of the stress values compared to the FE model. Based on this estimate, a parametric study was conducted for a range of

*Corresponding author.
E-mail address: lgz@buaa.edu.cn (Guozhu Liang).

Peer review under responsibility of National Laboratory for Aeronautics and Astronautics, China.

Production and hosting by Elsevier


http://dx.doi.org/10.1016/j.jppr.2013.01.002

rotational velocities under high temperature loads for a series of disc radii. Finally, it was found that this method can be used for the preliminary design of different turbines.


## 1. Introduction

Rotating discs are historically of interest to designers in the aerospace industry because of their vast range of uses. Gas turbine discs are an important example of such applications. In liquid rocket engines, rotating discs are simultaneously subjected to mechanical and thermal loads. A disc may be under internal pressure because of being shrink-fitted onto its mounting shaft. In addition, the blade effects installed on its outer periphery cause an external load to be applied to its outer edge. During operation, the disc rotates with a significant angular velocity as a result of the hot gases passing through the blades, which create a variable temperature field on the disc. In one study, a finite element (FE) analysis was performed to examine the damage mechanisms of a turbine disc, along with the critical high stresses caused by excessive rotational speeds [1]. Another study utilised an analytical solution to show the magnitudes of the circumferential stress components with respect to the radial stress components in a rotating disc [2]. Other studies used an analysis procedure based on modelling the disc as a series of connected constant thickness rings. In this investigation, the criterion of failure was shown to be the effective stress distribution at the state of yield [3]. Another analytical procedure was performed to evaluate the elastic stresses and strains on the disc [4,5]. Three-dimensional (3D) simulations of rotating metal discs were also used to evaluate the sensitivity of the disc stability to material parameters [6]. Furthermore, the axisymmetric deformations of a rotating disc with variable thickness were explored [7].

In this work, the FE technique was used to analyse the stresses and deformations caused by different types of loads, separate and combined. The stress results were compared using a simplified analytical routine.

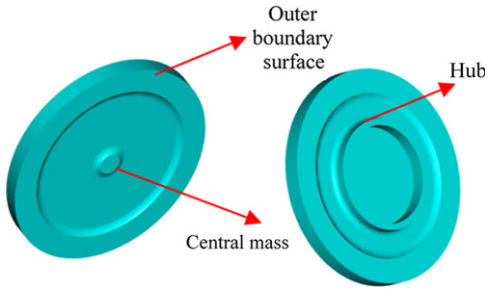


**Figure 1** Gas turbine disc.

## 2. Description of gas turbine disc

This section provides outlines of the disc geometry, material, and operating conditions.

### 2.1. Disc geometry

Figure 1 shows an illustration of the turbine disc under investigation. This turbine disc has a non-uniform thickness that varies from 0.008 m to 0.014 m, with an outer diameter equals to 0.180 m. The detailed dimensions of the non-uniform disc are shown in Figure 2. This disc also has a hub where the turbine shaft is attached.

### 2.2. Disc material

A chrome–nickel steel alloy is the current material used for the gas turbine discs. The material properties were taken to vary with temperatures from 0 °C up to 800 °C [8], as shown in Table 1.

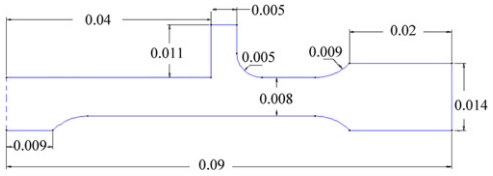


**Figure 2** Detailed dimensions of disc cross section (unit: m).

**Table 1** Engineering constants.

| Data | Temperature/°C | | | | | | |
|---|---|---|---|---|---|---|---|
| | 0 | 100 | 200 | 300 | 400 | 600 | 800 |
| $K$ | 22 | 22 | 22 | 22 | 24 | 24 | 26 |
| $\alpha/10^{-6}$ | 9.32 | 9.44 | 9.64 | 9.77 | 9.87 | 9.97 | 10.00 |
| Data | Temperature/°C | | | | | | |
| | 25 | 95 | 205 | 315 | 425 | 595 | 815 |
| $E$ | 200 | 195 | 185 | 175 | 166 | 154 | 136 |
| $v$ | 0.293 | 0.297 | 0.302 | 0.308 | 0.314 | 0.324 | 0.336 |

Where $E$: Young's modulus (GPa)
$v$: Poisson's ratio
$K$: Thermal conductivity (W/(m · °C))
$\rho$: Density, $\rho = 7835$ kg/m$^3$
$\alpha$: Coefficient of thermal expansion, $\alpha = 10 \times 10^{-6}$ °C
$C_P$: Specific heat, $C_P = 460$ J/(kg · °C)

### 2.3. Disc operating conditions

The turbine was operated at a rotational speed of 380 revolutions per second (rps) and a total power equal to 750 kW. The turbine blades, which were attached to the outer boundary surface of the disc, are not presented in Figure 1, but their mechanical and thermal effects on the disc were taken into consideration. The mechanical effect was a result of the total centrifugal force caused by the blades, which was simulated by a uniformly distributed pressure of 45 MPa (outward direction) at the outer boundary surface of the disc. This simplification ignores the stress concentration at the connection area between the disc and blades. Although it was appropriate in evaluating the strength of the disc, a 3D elastic–plastic analysis should be employed for a fatigue calculation for the blade. On the other hand, the thermal effect that originated from the attached hot blades was represented by an abrupt high temperature of 600 °C at the outer boundary surface of the disc. Because of thermal conduction, heat was transferred from the outer boundary surface to the centre of the disc for the subsequent 100 s, representing one operational life cycle of the turbine. For the torque transmission, the turbine shaft was shrink-fitted onto the disc hub. The amount of interference between the inner diameter of the hub and the outer diameter of the shaft was 0.0001 m and extended 0.01 m along the length of the hub. Analytically, this induced a contact pressure of 26 MPa. Although the shaft was also not shown, to assess the level of stresses arising from the shrink fit, this value was simulated as a pressure load on the inner surface of the hub.

## 3. Finite element modelling

### 3.1. Real turbine disc modelling

#### 3.1.1. Meshing

Because of the symmetry of the problem (loads and geometry), the disc was simulated by a two-dimensional (2D) axisymmetric cross-section. The disc was modelled using the commercial multi-purpose FE software package PATRAN. The geometry of the 2D non-uniform disc was meshed with six-node solid triangular elements having two translational degrees of freedom (DOF) per node (UX and UZ), and each having a global edge length of 0.002 m. The total number of elements used was 639. The mesh and element shape are illustrated in Figure 3.

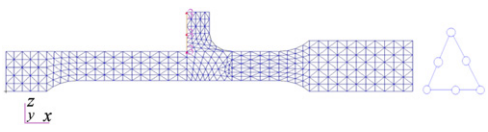


**Figure 3** Meshing of 2D non-uniform real disc model.

#### 3.1.2. Loads and boundary conditions

Four different types of loads were applied to the model: a rotational load, shrink-fitted load, blades' outer boundary load, and thermal load. The rotational load was simulated by an inertial velocity in the $z$-direction of 380 rps. The shrink fit load caused by the shaft is represented by a pressure of 26 MPa, and it was applied to the inner surface of the hub. The load from the blades was represented by a uniformly distributed pressure of 45 MPa at the outer boundary surface of the disc. Finally, the thermal load was represented by a temperature of 600 °C at the outer boundary surface of the disc. For symmetrical boundary conditions for the displacement of the disc, all of the nodes at the inner vertical surface of the hub were fixed in the $z$-direction, which represented the actual fixation method for the disc to the turbine shaft.

#### 3.1.3. Results and discussion

The PATRAN FE package was used to perform linear static analyses to solve five different load cases. These load cases were the rotational load (load case 1), shrink-fitted load (load case 2), blades' outer boundary load (load case 3), temperature gradient as a thermal load (load case 4), and combination of all the loads (load case 5). The results in terms of the Von Mises stress distributions are shown below.

- *Load case 1*
  For the rotational load, as shown in Figure 4, the maximum stress of 238 MPa occurred at the centre of the disc, and the maximum displacement of $5.20 \times 10^{-5}$ m occurred at the disc's outer radius. The shape of this deformation was caused by the hub.
- *Load case 2*
  For the shrink-fitted load, as shown in Figure 5, the maximum stress of 190 MPa occurred at the hub of the disc, and the maximum displacement of $7.60 \times 10^{-5}$ m occurred at the disc's outer radius.
- *Load case 3*
  For the blades' outer boundary load, as shown in Figure 6, the maximum stress of 89 MPa occurred at the lower surface of the disc, and the maximum displacement of $3.52 \times 10^{-5}$ m occurred at the disc's outer radius.
- *Load case 4*
  A thermal transient analysis was performed to define the temperature gradient along the disc at different time intervals during operation. Figure 7 shows the variation in the maximum thermal stresses with the operating time at three selected positions along the disc and the temperature variation at the centre of the disc over time under two different types of thermal loads: conduction only and conduction plus convection. These three positions were at the centre ($r = 0$ m), middle ($r = 0.045$ m), and outer radius ($r = 0.09$ m) of the disc. A transient thermal analysis was conducted not only for 100 s, which represented

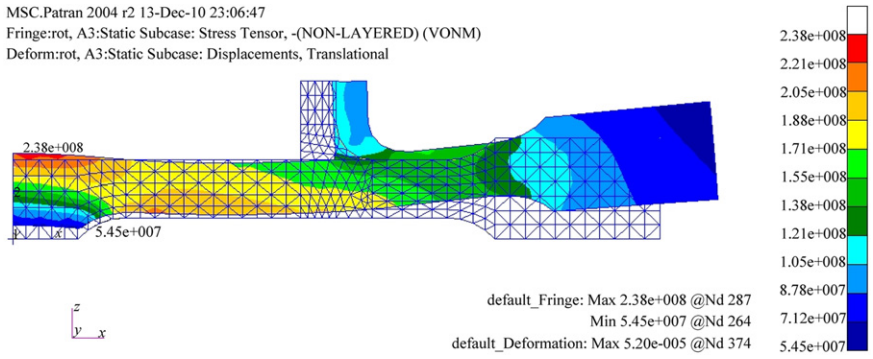


**Figure 4** Load case 1: rotational load.

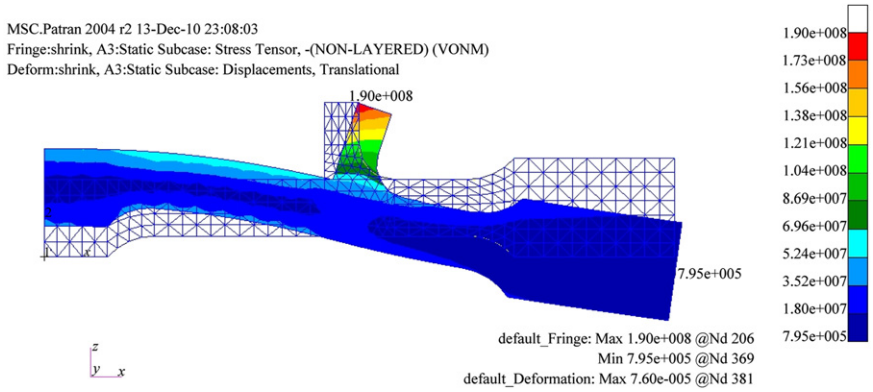


**Figure 5** Load case 2: shrink-fitted load.

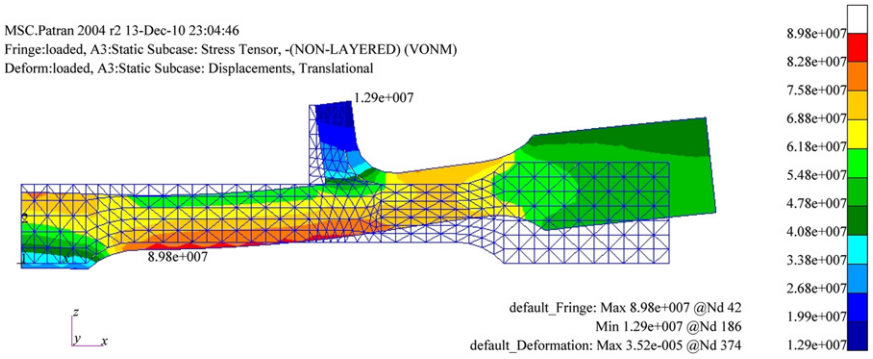


**Figure 6** Load case 3: blades' outer boundary load.

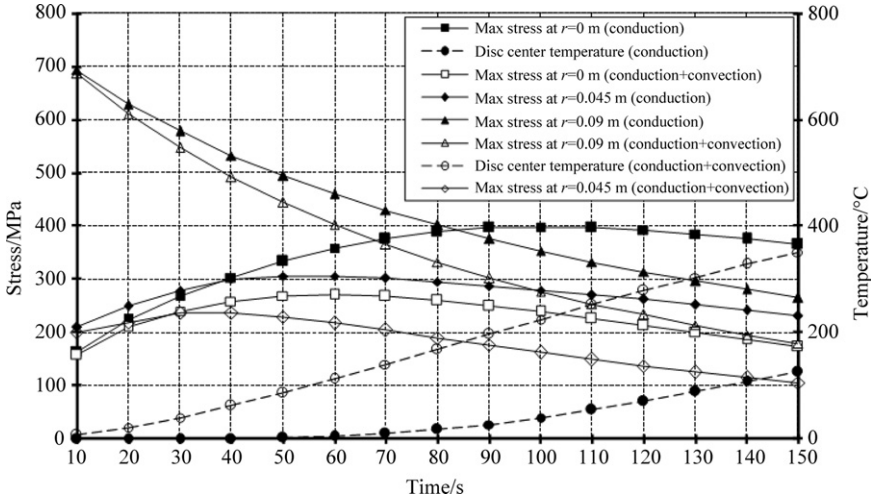


**Figure 7** Thermal stress along disc and temperature of disc's centre under conduction and convection.

one life cycle of the turbine, but also extended for 150 s to study the behaviour of the stresses for a longer operating time. First, from the conduction heat transfer mode shown in this figure, it is clear that during the first 10 s, the value of the thermal stress at the outer radius of the disc was 694 MPa. This value was much higher than the value at the centre because of the concentration of excess heat in only 0.02 m of the disc from the outer boundary surface, as shown in Figure 8. Then, as time passed, this heat was conducted and distributed along the disc. Therefore, the value of the stress at the outer radius decreased until reaching the value of 350 MPa at the end of the operating time. Furthermore, the stress at the disc's centre started with a small value of 162 MPa and increased to a maximum value of 399 MPa at 100 s before decreasing. In addition, at the disc's middle point, the stress started with a value of 180 MPa, increased to a maximum value of 306 MPa at 60 s, and then decreased. In addition, the temperature of the disc's centre remained at 0 °C for the first 40 s and then steadily rose to 45 °C at 100 s. It then increased until reaching its steady state. Second, for the convection heat transfer mode

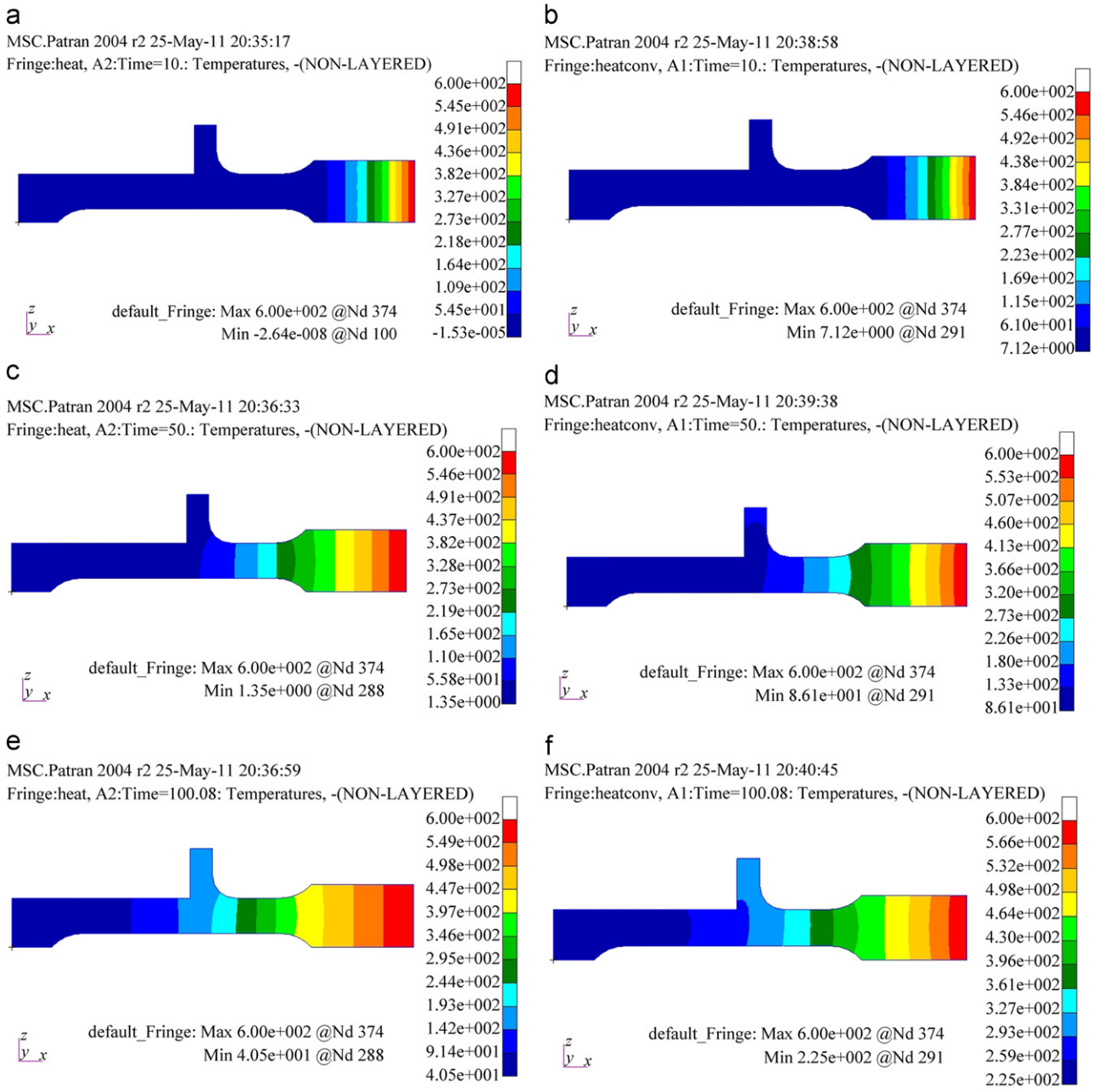


**Figure 8** Temperature distributions in disc at different operating times under conduction and convection. (a) Time = 10 s (conduction), (b) time = 10 s (conduction+convection), (c) time = 50 s (conduction), (d) time = 50 s (conduction+convection), (e) time = 100 s (conduction) and (f) time = 100 s (conduction+convection).

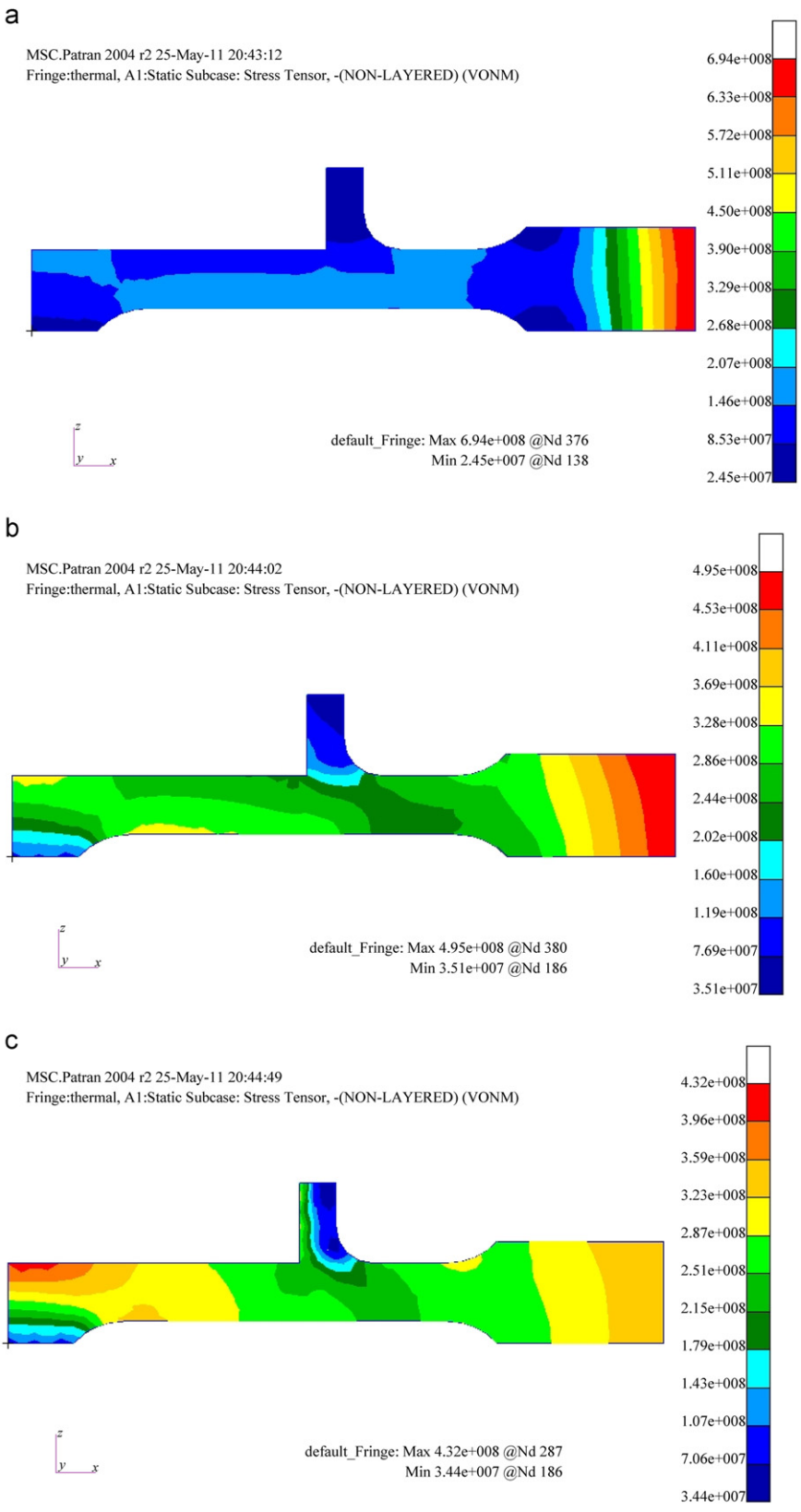


**Figure 9** Load case 4: thermal load at different operating times under conduction only. (a) Time = 10 s (conduction), (b) time = 50 s (conduction) and (c) time = 100 s (conduction).

combined with the conduction to analyse the effect of using another type of heat transfer mode on the stresses, it was assumed to be a forced convection mode with a convection coefficient $h = 200\ \mathrm{W/(m^2 \cdot {}^\circ C)}$, and the temperature of the hot gases surrounding the disc during its operation was 200 °C. Actually, under real operating conditions, these values will be larger because of the high rotation speed of the turbine in a hot medium. Therefore, these assumed values were acceptable for the analysis.

An inspection of the curves in Figure 7 shows that the behaviour of the change in the thermal stresses is the same in both modes, but a lower value is seen in the convection mode. This reduction in the stress level for all of the points along the disc was caused by the excess quantity of heat that had been added from the surrounding hot gases to the disc by convection, which increased the rate of temperature change for all of the points. This decreased the temperature gradient and therefore reduced the thermal stresses. Based on this, the temperature of the disc's centre remained at 0 °C for the first 5 s, and then, it steadily rose to 225 °C at 100 s. The stress at the disc's centre reached its maximum value at 60 s, which is shorter than the time in the case of conduction only. This was also repeated at the disc's middle point, where the maximum value was reached at 40 s. It was noticed that the conduction mode played the predominant role in affecting the stresses all over the disc. From this point of view, Figure 9 shows the thermal load of the disc at three different times—10 s, 50 s, and 100 s—to represent the state of stress at the beginning, midway through, and end of the operation, respectively when utilising the conduction heat transfer mode only.

- *Load case 5*

  The combination of four different loads (load case 5) was applied to the model at the start and end of the operation (10 s and 100 s), using the maximum conduction thermal load. The results for the stress and displacement are shown in Figures 10–12. Based on the FE results, the maximum stresses for the different load cases were tabulated. Table 2 summarises the values and positions of the maximum Von Mises stresses applied to the disc and the maximum displacements caused by different types of loads at the end of 100 s. It is observed from this table that the thermal load had the greatest effect on the disc. The maximum stress caused by the thermal load

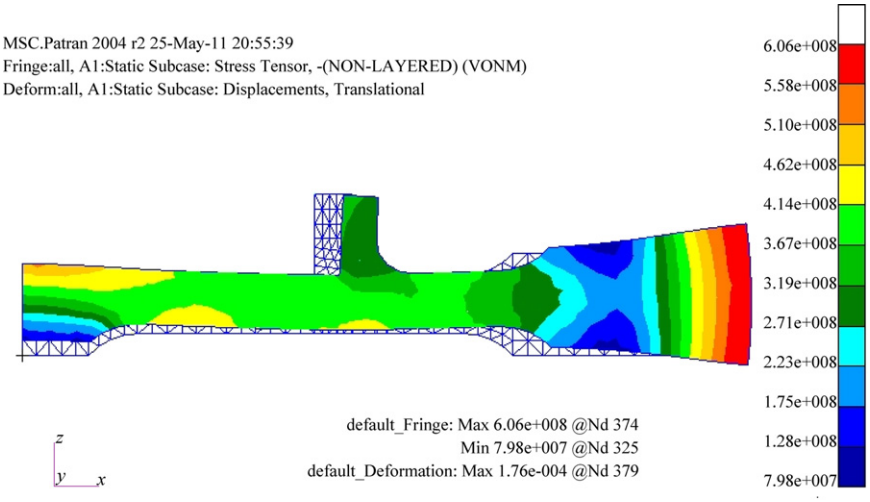


**Figure 10** Load case 5: stress caused by rotation, shrink fitting, blades, and conduction thermal loads at 10 s.

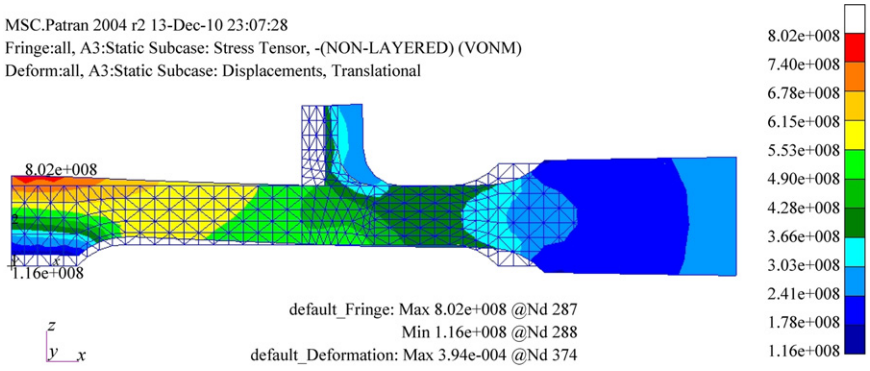


**Figure 11** Load case 5: stress caused by rotation, shrink fitting, blades, and conduction thermal loads at 100 s.

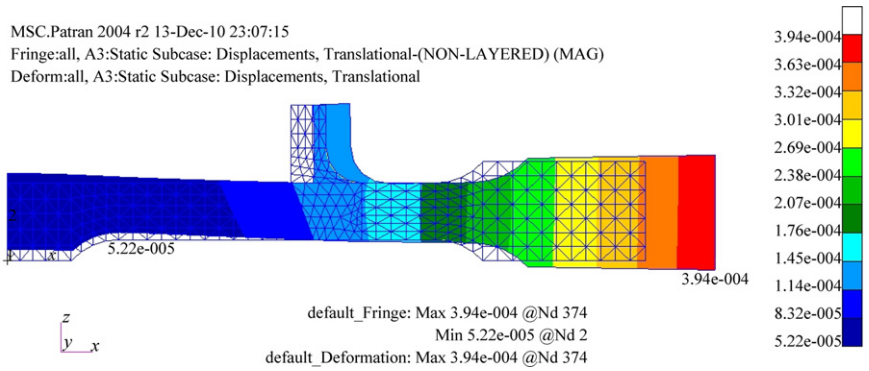


**Figure 12** Load case 5: displacement caused by rotation, shrink fitting, blades, and conduction thermal loads at 100 s.

**Table 2** Maximum stresses and displacements caused by different loads at 100 s.

| Type of loads | Max stress /MPa | Position of max stress | Max displacement /m | Position of max displacement |
|---|---|---|---|---|
| Rotation (load case 1) | 238 | Disc centre | $5.20 \times 10^{-5}$ | Disc outer radius |
| Shrink fitted (load case 2) | 190 | Disc hub | $7.60 \times 10^{-5}$ | Disc outer radius |
| Blades' outer boundary (load case 3) | 89 | At radius $r=0.02$ m | $3.52 \times 10^{-5}$ | Disc outer radius |
| Thermal (load case 4) | 432 | Disc centre | $3.32 \times 10^{-4}$ | Disc outer radius |
| Combining all the loads (load case 5) | 800 | Disc centre | $3.94 \times 10^{-4}$ | Disc outer radius |

accounted for about 50% of the maximum stress from all the loads (Figure 11).

In addition, the maximum stress caused by the rotation load was about 25% of the total maximum stress. The maximum stresses for the rotational and thermal loads occurred at the centre. Moreover, for the shrink-fitted load, the maximum stress values were totally localised in the hub. On the other hand, as shown in Figure 10, for the first 10 s of operation, a maximum stress of 600 MPa was observed at the outer radius of the disc. The real operating conditions represented in load case 5 proved that the maximum stresses also occurred at the disc's centre. These detailed stress analyses for a disc subjected to different types of loads show the importance of using FE analysis in simulating a real design case because it takes into consideration the non-uniform complex shape and real operating conditions.

## 3.2. *Effect of mass removal from disc on stresses*

The main reason in using a non-uniform disc thickness is to reduce the weight of the turbine. Weight is a major parameter for optimisation when designing and manufacturing turbine discs. Because removing material will mainly affect the rotational load, the rotational load was simulated using an inertial velocity in the $z$-direction of 380 rps, and it was the only load applied for all of these models. In addition, the same element type, shape, material properties, and boundary conditions were used as those in the non-uniform real disc model. To study the effect of mass removal on the stresses when using a non-uniform disc thickness, the following four models were analysed.

- *Disc with uniform thickness*
  Figure 13 shows a uniform disc. Because of the symmetry of the problem (loads and geometry), this uniform disc was simulated using a 2D rectangle, in which the length of the rectangle represents the radius (0.09 m) of the disc, while the height of the rectangle represents its thickness (0.014 m). The maximum stress at the disc's centre was 194 MPa, the deformation was in the radial direction, and the stresses were distributed uniformly along the disc's radius.
- *Disc with two thicknesses*
  Figure 14 shows a disc with a thickness step from 0.014 m to 0.008 m. The maximum stress at the disc's centre was 189 MPa, and the deformation was in the radial direction.
- *Disc with two thicknesses and a hub*
  Figure 15 shows a disc with a thickness step from 0.014 m to 0.008 m and a hub. The maximum stress at the disc's centre was 196 MPa, and the deformation was in the radial direction but bent towards the hub.
- *Disc with two thicknesses and a central mass*
  Figure 16 shows a disc with a thickness step from 0.014 m to 0.008 m and a central mass. The maximum

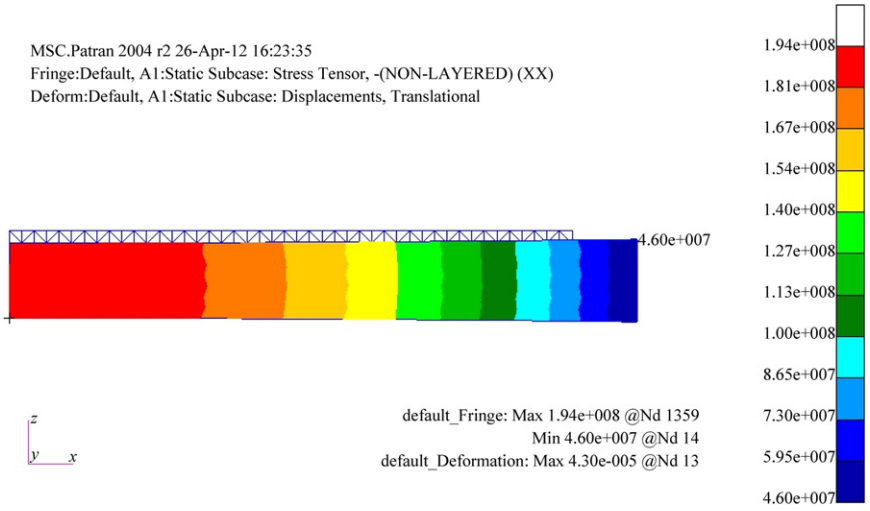


**Figure 13** Radial stresses with deformed shape caused by rotational loads for uniform disc.

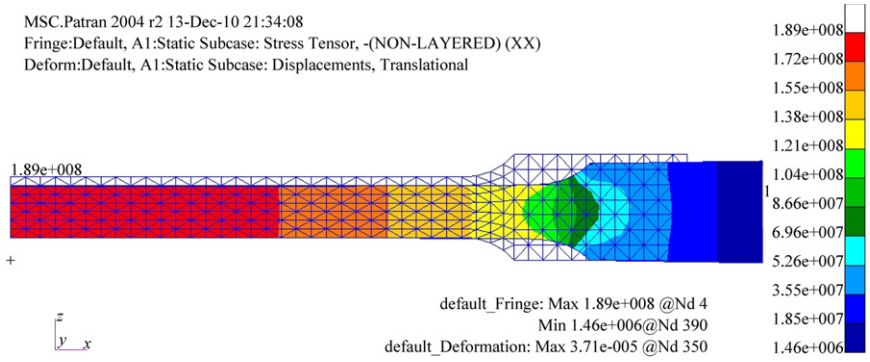


**Figure 14** Radial stresses with deformed shape for disc with two thicknesses.

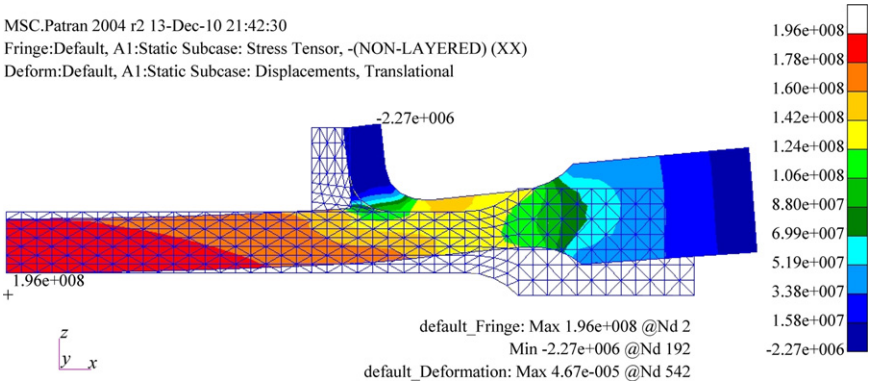


**Figure 15** Radial stresses with deformed shape for disc with two thicknesses and hub.

stress at the disc's centre was 244 MPa, and the deformation was in the radial direction.

Table 3 summarises the masses of the different disc geometries and the corresponding maximum stresses and displacements caused by the rotational load. From this table, it is clear that the difference in mass between the discs with the uniform and non-uniform thicknesses was about 0.5 kg, and this mass removal resulted in an increase in the stress of about 25%. Moreover, the central mass had the main influence on the high stress values at the disc's centre. In addition, the hub caused the direction of deformation of the disc to be bent towards the hub, with a maximum displacement of $4.67 \times 10^{-5}$ m. Finally, the FE model revealed that reducing the weight of the disc by using a non-uniform thickness should be optimised.

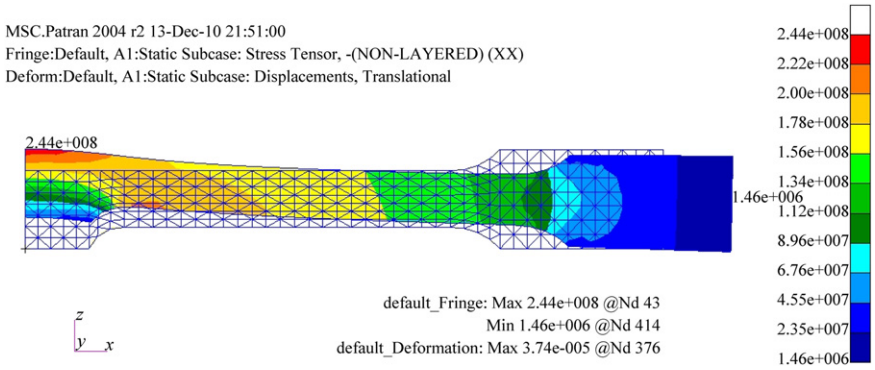


**Figure 16** Radial stresses with deformed shape for disc with two thicknesses and central mass.

**Table 3** Effect of mass removal from disc on stress and displacement caused by rotational load.

| Model | Mass/kg | Max stress at centre/MPa | Max displacement/m |
|---|---|---|---|
| Disc with non-uniform thickness (refer to Figure 4) | 2.24 | 238 | $5.20 \times 10^{-5}$ |
| Disc with uniform thickness | 2.79 | 194 | $4.10 \times 10^{-5}$ |
| Disc with two thicknesses | 2.10 | 189 | $3.71 \times 10^{-5}$ |
| Disc with two thicknesses and a hub | 2.23 | 196 | $4.67 \times 10^{-5}$ |
| Disc with two thicknesses and a central mass | 2.11 | 244 | $3.74 \times 10^{-5}$ |

**Table 4** Analytical results for solid uniform disc.

| Radius $r$/m | Rotational load | | Thermal load | | Rotational and thermal loads | |
|---|---|---|---|---|---|---|
| | $\sigma_r$/MPa | $\sigma_\theta$/MPa | $\sigma_r$/MPa | $\sigma_\theta$/MPa | $\sigma_r$/MPa | $\sigma_\theta$/MPa |
| 0 | 197 | 197 | 412 | 412 | 564 | 564 |
| 0.09 | 45 | 109 | 45 | −322 | 45 | −256 |

## 4. Simple method to predict stresses of turbine disc

### *4.1. Analytical solution for stress in thin rotating solid uniform disc*

A simple method is proposed to predict an approximate value for the stresses in a thin uniform turbine disc. This method would be a good tool and a simple way to assist designers in the preliminary design step to determine the level of stress in a disc, which would allow them to choose the most suitable material for it. From the detailed study of the FE stress analysis of the non-uniform real disc and according to Table 2, it was clear that the main loads affecting the disc are the rotational and thermal loads. Based on these results, the use of just these loads is acceptable for a preliminary disc design.

The applied load on the disc is a combination of rotational and thermal loads. For a thin disc rotating at a constant speed, the stresses and deformations induced by the centrifugal forces are symmetrical about the $z$-axis. Because the disc is thin, the radial and hoop stresses are constant throughout the thickness. Thus, there are no stresses in the $z$-direction. On the other hand, because of the non-uniform temperature distribution within the disc, thermal stress components would develop along the radial and circumferential directions. The stress distributions caused by combining the rotational and thermal loads are represented by using the following formulas available in textbooks [9,10]:

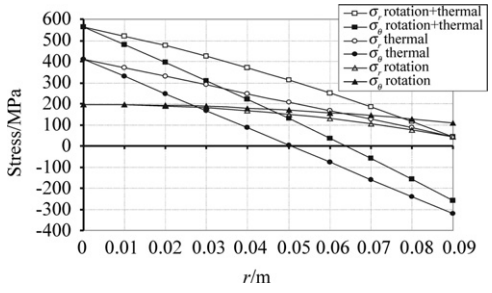


**Figure 17** Radial and hoop stresses caused by rotational and thermal loads for solid uniform disc.

$$\sigma_r = A - \frac{B}{r^2} - \left(\frac{3+v}{8}\right)\rho\omega^2 r^2 - \frac{\alpha E}{r^2}\int Tr\,\mathrm{d}r \tag{1}$$

**Table 5** Comparison between FE for non-uniform disc and analytical solution for uniform disc.

| | Rotational load/MPa | Thermal load/MPa | Rotational and thermal loads/MPa |
|---|---|---|---|
| FE for non-uniform disc | 238 | 432 | 800 |
| Analytical solution for uniform disc | 197 | 402 | 551 |

$$\sigma_\theta = A + \frac{B}{r^2} - \left(\frac{1+3v}{8}\right)\rho\omega^2 r^2 + \frac{\alpha E}{r^2}\int Tr\,\mathrm{d}r - \alpha E T \qquad (2)$$

where $A$ and $B$ are constants found from the boundary conditions, $r$ is the radius, $\omega$ is the rotational speed, $\sigma_r$ is the stress in the radial direction, $\sigma_\theta$ is the stress in the hoop direction and $T$ is the temperature.

If the disc is continuous from the centre to the outer radius, then it is apparent that, unless $B=0$, the stresses would become infinite at $r=0$, so that constant $B$ must be equal to 0. To find constant $A$, it is necessary to use the boundary condition at the outer radius where $\sigma_r=0$ in the case of a solid disc with an unloaded outer boundary (no blades are attached to the disc). However, for loaded boundary conditions, if a number of blades are attached to the outer radius of the disc, each of these has a centrifugal force component, which will be present at the outer periphery of the disc. Given the mass of each blade, its effective centre of mass and the number of blades, we can now compute the total centrifugal force as a uniformly distributed load. Dividing this total centrifugal force by the thickness of the outer boundary area provides the value of stress in the radial direction at the outer radius of the disc, in this case $\sigma_r \neq 0$. In our case, for a disc with a loaded boundary at outer radius $r=0.09$ m, the radial stress is $\sigma_r=45$ MPa, and the rotational speed $\omega=380$ rps.

For the thermal gradient, it is assumed that the temperature variation along the disc is linear, having the form $T=ra+b$, where $a$ and $b$ are constants found from the temperature boundary conditions. In our case, it is assumed that the temperature is equal to 50 °C at $r=0$ and is equal to 600 °C at $r=0.09$ m. The temperature constants can be calculated to be $a=6111$ °C and $b=50$ °C. Finally, the integration for the linear temperature distribution along the disc is computed from $r=0$ m to $r=0.09$ m to be $[ar^3+0.5br^2]$. Thus, the stress distributions caused by the rotational and thermal loads (separately and combined) can be calculated using the same formula. Table 4 shows the values of the radial and hoop stresses caused by these loads, where $T=0$ in the case of applying the rotational load only and $\omega=0$ in the case of applying the thermal load only. The results are demonstrated in Figure 17, which shows that the thermal loads are higher than the rotational loads, the maximum stress caused by the rotational load is at the disc's centre, the maximum stress caused by the thermal load is at the disc's centre and the maximum stress caused by combining the two loads is also located at the disc's centre, with a value of 564 MPa.

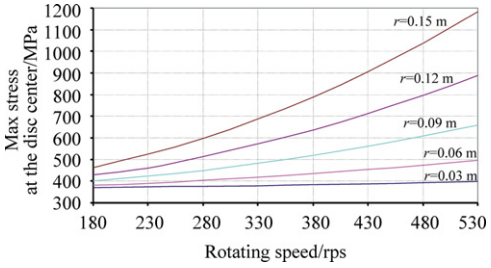


**Figure 18** Stresses in steel solid uniform disc caused by rotational and thermal loads at 550 °C temperature gradient between disc centre and outer radius.

Table 5 compares the FE results for the non-uniform disc and the analytical solution for the uniform disc under rotational and thermal loads, where all of the stress values were obtained at the disc's centre. An inspection of these values reveals that the simple analytical method compares favourably with the FE results for the separate rotational and thermal loads. On the other hand, when combining the rotational and thermal loads, it is shown that the stresses derived with the analytical method are about 30% smaller than the FE results, which proves that the simple analytical method gives a good prediction of the stress level for the disc in the earlier design step.

### *4.2. Parametric study to obtain stresses for thin rotating solid uniform disc*

Eqs. (1) and (2) were solved under rotational and thermal loads with variations in the rotational velocity (180–530 rps) and disc radius (0.03–0.15 m). The resulting curves shown in Figure 18 serve as a guide for preliminary design to estimate the maximum stresses at the disc's centre caused by rotational and thermal loads for a uniform solid disc.

## 5. Conclusions

This paper presented an FE analysis of the stresses and deformations developed in a gas turbine disc used in a liquid rocket engine. A 2D axisymmetric disc was created using general-purpose FE software for analysis. The results were compared with a simplified analytical

solution that gave approximate values for the stresses at the disc.

The 2D disc modelling was quite adequate as a demonstration of a real disc taking into consideration all of the applied loads. Several load cases were investigated to assess the relative contribution of the various loads imposed on the turbine during operation, namely, the stresses caused by the rotational load, blades' outer boundary load, shrink-fitted load, and temperature gradient as a thermal load. A linear static analysis and transient thermal analysis were conducted, taking into consideration the material behaviour at elevated temperatures. In addition, the deformations of the disc caused by different types of loads and the shape of the disc were studied. The effect on the stresses of removing mass from the disc to reduce its weight was presented and showed an increase in stress of about 25%.

Finally, conduction was found to be the most severe heat transfer mode for the disc, but convection increased the rate of temperature change and could potentially lead to a less severe temperature gradient across the disc. In addition, an inspection of the results revealed that the deformation occurred in the radial direction except when modelling the hub. In that case, the direction of deformation was bent towards the hub. It was also observed that the greatest stresses in the disc resulted from the thermal loads. The thermal stresses on the disc were quite high because of the sharp temperature gradient that existed in the turbine disc. For the present design, the stresses at the disc's centre were shown to be higher than those at any other area of the disc.

## References

[1] L. Witek, Failure analysis of turbine disc of an aero engine, Engineering Failure Analysis 13 (1) (2006) 9–17.
[2] H. Callioglu, M. Topcu, A. Tarakcilar, Elastic–plastic stress analysis of an orthotropic rotating disc, International Journal of Mechanical Sciences 48 (9) (2006) 985–990.
[3] H. Jahed, B. Farshi, J. Bidabadi, Minimum weight design of inhomogeneous rotating discs, International Journal of Pressure Vessels and Piping 82 (1) (2005) 35–41.
[4] V. Vullo, F. Vivio, Elastic stress analysis of non-linear variable thickness rotating discs subjected to thermal load and having variable density along the radius, International Journal of Solids and Structures 45 (20) (2008) 5337–5355.
[5] M.H. Hojjati, A. Hassani, Theoretical and numerical analyses of rotating discs of non-uniform thickness and density, International Journal of Pressure Vessels and Piping 85 (10) (2008) 694–700.
[6] M. Maziere, J. Besson, S. Forest, Overspeed burst of elastoviscoplastic rotating discs, part I: analytical and numerical stability analyses, European Journal of Mechanics A/Solids 28 (1) (2009) 36–44.
[7] G.J. Nie, R.C. Batra, Stress analysis and material tailoring in isotropic linear thermoelastic incompressible functionally graded rotating discs of variable thickness, Composite Structures 92 (3) (2010) 720–729.
[8] C.L. Clark, High Temperature Alloys, Pitman, New York, 1993.
[9] A.R. Ragab, S.A. Bayoumi, Engineering Solid Mechanics, CRC Press, Boca Raton, FL, 1999.
[10] P.P. Benham, R.J. Crawford, Mechanics of Engineering Materials, John Wiley and Sons, New York, 1987.